Nanoscale

Accepted Manuscript

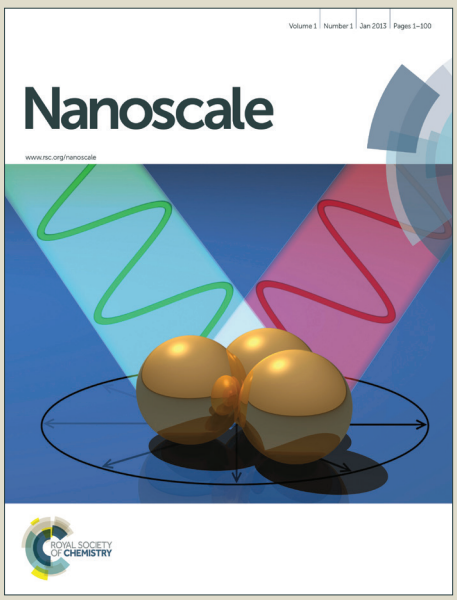

ROYAL SOCIETY OF CHEMISTRY

www.rsc.org/nanoscale

CdSe-CdS Quantum Dots Co-Sensitized ZnO Hierarchical Hybrids for Solar Cells with Enhanced Photo-Electrical Conversion Efficiency

Zhimin Yuan, Longwei Yin*

Key Laboratory for Liquid-Solid Structural Evolution and Processing of Materials, Ministry of Education, School of Materials Science and Engineering, Shandong University, Jinan 250061, P. R. China

*To whom correspondence should be addressed. Tel.: + 86 531 88396970. Fax: + 86 531 88396970. E-mail: yinlw@sdu.edu.cn

ABSTRACT

We have developed a facile method to fabricate CdSe-CdS quantum dots sensitized hierarchical ZnO nanostructures for quantum dots sensitized solar cells (QDSCs) by combining hydrothermal method, successive ionic layer adsorption and chemical reaction techniques (SILAR). The method consists of the growth of ZnO hierarchical structure on ITO substrates via a hydrothermal method and the layer deposition of double quantum dots CdSe and CdS by SILAR. The CdSe-CdS QDs co-sensitized ZnO hierarchical structures show enhanced light absorption in entire visible light range. The photovoltaic performance of QDCSs based on CdSe-CdS QDs co-sensitized ZnO hierarchical structures was evaluated. As photoanodes for QDSCs, the CdSe-CdS QDs double-sensitized ZnO hierarchical structures demonstrate an increased J_{sc} and improved power conversion efficiency up to 1.39%. Under light illumination, photons are captured by QDs, yielding electron-hole pairs that are rapidly separated to electrons and holes at the interface between the ZnO and the QDs. The electrons are transferred to the conduction band of ZnO and the holes are released by redox couples in the liquid polysulfide (S^{2-}/S_x^{2-}) electrolyte, resulting in greatly improved photo-electrical conversion efficiency of QDSCs. The results suggest that it is very promising and feasible to enhance light absorption, carrier generation, and effective carrier separation via band engineering by CdSe-CdS QDs co-sensitization, and the method reported here displays a great potential applications to be scaled up.

1. Introduction

Quantum dot sensitized solar cells (QDSCs), as a derivative of dye-sensitized solar cells (DSSCs), have attracted worldwide scientific and technological interest since the breakthrough work of colloidal TiO_2 based DSSCs by O'Regan and Grätzel in 1991[1] for the lower cost compared to silicon-based traditional solar cells.[2,3] Typical DSSCs consist of TiO_2 mesoporous photoanodes, a dye sensitizer, and electrolyte.[4] To enhance light harvest in the visible light region, many efforts have been made to focus on the development of high performance sensitizers.[5-8] It is still a challenge to obtain an ideal organic dye as sensitizer to absorb photons in the full sunlight spectra. For this reason, another alternative selection for the sensitizer is narrow-band gap semiconductor quantum dots (QDs), such as CdS,[9,10] CdSe,[11,12] PbS,[13] and InAs,[14] which present extraordinary optical and electrical properties over traditional organic dyes, have been paid particular attention recently due to the tenability of chemical composition, crystal structure, size and optical responsibility. In comparison with organic molecular dyes, inorganic semiconductor QDs are considered as highly promising next-generation sensitizers due to the following advantages over dyes:[15-21] (1) easy tuning of the optical band-gap energy through controlling the size and composition of QDs; (2) larger extinction coefficient, enabling the device thickness to be thinner; (3) higher stability toward water and oxygen; (4) possibilities of generating multiple excitons from single-photon absorption, through the impact ionization effect (or inverse Auger process), which could push the theoretical maximum conversion efficiency of these devices as high as 44%.[22-24]

In order to increase the efficiency of QDSCs, 3D hierarchical semiconductor architecture matrices are generally utilized to serve as a scaffold to hold the QDs and thus to increase the effective surface area of cell.[25,26] The 3D hierarchical semiconductor architectures can effectively serve as the photoelectrodes to collect the photogenerated carriers more efficiently. Compared with TiO_2, ZnO is of great importance because of their unique electrical and optical properties, and ZnO nanostructure can be grown easily over a large area by a variety of methods, such as template synthesis (3D structures),[27,28] and layer-by-layer fabrication (2D structures).[29,30] We also can utilize electrospining method used in $Li_4Ti_5O_{12}$[31,32] (1D structures) to obtain ZnO nanostructure. In particular, QDSCs based on ZnO arrays of nanorods, nanowires, nanocables grown on a conducting substrate have been reported.[33] It has been shown that ZnO nanorod arrays could provide a direct current pathway for electrons to the external circuit with few grain boundaries.[34] The array configuration of ZnO nanostructures could enhance light absorption due to scattering and trapping,[35] which may benefit the enhancement of photo-electric conversion efficiency. Nobel metals, such as Pt and Au, generally used as the counter electrode materials in DSSCs, are inefficient in S^{2-}/S_x^{2-} in QDSCs, because their surface activity toward interaction with the polysulfide redox couple is poor.[36] Various materials have

been investigated as the counter electrode of QDSCs, including CoS,[36,37] CuS,[37] CuS/CoS,[38] Cu_2S,[36,39,40] and carbon based fabric (nanotube,[41] graphite,[42] carbon black,[43] and mesoporous carbon[44]). Hodes et al. reported that Cu_2S acts as a suitable electrocatalyst for the S^{2-}/S_x^{2-} redox reaction.[36]

Narrow band gap chalcogenide quantum dots sensitization using CdS, CdSe, CdTe, and ZnSe QDs for wide band gap semiconductors (ZnO, TiO_2, SnO_2) are proven to be effective to enhance the photo-electrical conversion efficiency of QDSCs via facilitating charger transfer, decreasing the recombination rate of photo-induced electrons and holes, extending the light absorption to visible region from ultraviolet region.[45,46] Thus far, power conversion efficiency around 2% has been reported for the double-sensitized ZnO nanostructure-based QDSSCs.[47-49] Wang's[50] study shows that the optical absorption of ZnO nanowire arrays can be tuned to the wavelength region up to 650 nm via double-sensitization with CdS and CdSe QDs, exhibiting higher photocatalytic activity as photoanodes for water splitting using a single white light source. It is revealed that: (i) The introduction of CdSe could extend the absorption edge drastically from <512 nm to >700 nm. (The band gap energy of CdS and CdSe is 2.42 and 1.74 eV, respectively.)[17,27] (ii) The alignment of the conduction and valence bands of CdSe with respect to those of CdS enables efficient separation and transfer of the photogenerated carriers. (iii) The CdS interlayer can serve as a passivation layer to inhibit the recombination of percolated electrons in the 1D ZnO nanostructures and oxidizing species in the electrolyte.[50] So, the CdSe and CdS QDs co-sensitization is of great importance for improving the photovoltaic performance of ZnO.

Several growth techniques have been developed for the QDs sensitization of ZnO nanostructures, such as direct growth by chemical bath deposition (CBD),[51] successive ionic layer adsorption and reaction (SILAR),[52] assembly of QDs by immobilization via organic linkers,[53] and electrochemical deposition method.[54] For the two types of QDs double-sensitized ZnO nanostructures, as an example, a common feature is that CdS QDs were grown by CBD on ZnO nanowires; then, the CdSe QDs were assembled on CdS QDs-sensitized ZnO nanowires by chemical modification to form a CdS/CdSe double-sensitized structure.[49] The method is complex, and it is difficult to uniformly control the chemical composition, thickness of CdS and CdSe on the surface of ZnO nanostructures over a large area due to easy aggregation of QDs.

In this work, we report a facile and low-cost SILAR approach to synthesize CdSe-CdS QDs double-sensitized hierarchical ZnO nanostructured architectures on indium-doped tin oxide (ITO)-coated glass substrates. The double-sensitized ZnO hierarchical structures show enhanced light absorption in entire visible light range. The photovoltaic performance of the double-sensitized ZnO hierarchical structure in photoelectrochemical solar cells was evaluated. The QDSCs based on the CdSe-CdS QDs double-sensitized ZnO hierarchical structures demonstrate

an increased J_{sc} and improved power conversion efficiency up to 1.39%. The results suggest that it is very promising and feasible to enhance light absorption, carrier generation, and effective carrier separation via band engineering by double QDs sensitization, and the method reported here displays a great potential to be scaled up.

2. Experimental

2.1 Materials preparation

2.1.1 Preparation of ZnO hierarchical structure

The ZnO hierarchical structure were synthesized via a facile one-step hydrothermal reaction according to the procedure reported in literature.[55] Commercial ITO slide glass was cut into 15×15 mm^2 slides as substrates for the direct deposition of ZnO and then carefully cleaned in ethanol and deionized water. The typical experimental details are described as follows: 40 mL aqueous solutions of 0.035 M $Zn(CH_3COO)_2 \cdot 2H_2O$ and 0.55 M NaOH were prepared using distilled water with stirring. The mixture precursor solution was added to a 80 mL Teflon-lined stainless steel autoclave. A piece of pretreated ITO glass was then immersed in the precursor solution before sealing, keeping the conductive glass surface upwards. The autoclave was kept at 70 °C for 12/24 h. Finally, the ITO glass was taken out of the solution, rinsed with distilled water several times and dried in air. Other experiments with different amounts of NaOH were performed.

2.1.2 Growth of CdS and CdSe QDs layers on the ZnO hierarchical structures

After calcination at 200°C for 30 min, the ZnO hierarchical structures were sensitized in situ with CdS and CdSe using SILAR. Scheme 1 shows deposition process of CdS and CdSe QDs on ITO/ZnO film. For CdS QD self-assembly, the ZnO electrodes were first immersed in an ethanol solution of MPA (0.3 M) for 12 h at 50°C. Pre-treatment of MPA modification on the ZnO hierarchical structure surface can facilitate the CdS QD adsorption. In order to deposit a CdS layer, ZnO hierarchical structure was successively immersed into four different solutions for 30 s each, which includes 0.1 M $Cd(NO_3)_2 \cdot 4H_2O$ in ethanol, pure ethanol, 0.2 M $Na_2S \cdot 9H_2O$ in methanol and pure methanol, respectively. Then the ZnO hierarchical structures film was rinsed with pure ethanol for 30 s or longer to remove excess precursor before the next dipping. The above process as illustrated in Fig. 1a was considered as one SILAR cycle and denoted as 1CdS. Different cycles were repeated according to the requirement of the CdS layer thickness. The deposition of the CdSe layer was similar to that of the CdS layer except for that Na_2S in methanol solution was replaced by Na_2Se in ethanol solution. Here, the sodium selenide (Na_2Se) solution was prepared in situ reaction of $NaBH_4$(0.1 M) and SeO_2(0.05 M) in methanol under the protection of N_2. All the electrodes analyzed in this study have been coated with ZnS passivation layer, carried out by one SILAR cycle consisting of twice dipping alternatively in the 0.1 M $Zn(NO_3)_2$ and 0.2 M Na_2S solutions for 1 min per dip. The

ZnO/CdS/CdSe substrates were then annealed at the 450°C for 30 min.

2.1.3 Preparation of the Cu_2S counter electrodes

Cu_2S formed on a brass sheet was used for counter electrode. Brass foil was etched in hydrochloric acid at 75°C for 15 min and subsequently washed with DI water and dried using air gun. Polysulfide solution composed of 1 M Na_2S, 1 M S and 0.5 M NaOH in pure ethanol was dropped on unmasked area of etched brass and black colored Cu_2S immediately formed on the brass foil.

2.2 Solar cell fabrication

Scheme 2 shows the sketch of the photoelectrical conversion structure of a QDSSC. The CdS and CdSe QDs sensitized ZnO working electrode and the Cu_2S-brass counter electrode were assembled using Surlyn (ca. 60mm) as a spacer and sealant. Polysulfide redox electrolyte was injected through the 0.75 mm-diameter hole at working electrode and the holes were sealed using Surlyn. For the best performance, 0.05 M of GuSCN was added to electrolyte. The area of the cells was 0.16 cm^2.

2.3 Characterization

The absorption and photoluminescence (PL) spectra were recorded using conventional spectrometers (Hitachi U-4100 and Cary-50. Varian Co., respectively). The purity and phase structure of materials were characterized by a Rigaku model Ru-200b X-ray powder diffractometer (XRD) equipped with Cu Ka radiation(λ=1.5406 Å). The morphology and components of the synthesized products were analyzed using SU-70 field emission scanning electron microscopy (FE-SEM) and attached energy-dispersive X-ray spectroscopy (EDS), respectively. The selected-area electron diffraction (SAED) characterization and microstructural analyses were carried out in a Phillips Tecnai 20U-Twin high-resolution transmission electron microscope at an acceleration voltage of 200 kV. Cells were tested using a solar simulator (Newport, Class 3A, 94023A) at one sun (AM1.5G, 100mW/cm^2) by a Keithley 2420 source meter equipped with a calibrated Si-reference cell (certificated by NREL).

3. Results and discussion

3.1 Structure and morphology characterization

Fig. 1 displays the SEM images of the ZnO products prepared in the presence of 0.55 M NaOH for different growth times of 12 h and 24 h, respectively, using 0.035 M $Zn(CH_3COO)_2 \cdot 2H_2O$ as a Zn precursor. For the ZnO products synthesized for 12 h, three-dimensional (3D) hierarchical architectures can be clearly revealed in Fig. 1a. A close observation in Fig. 1b indicates that the 3D hierarchical nanostructure is composed of rod-like crystals of 300-350 nm in diameter and a length of 4-5 μm (aspect ratio ~ 14) radiated from the center. Fig. 1c presents the cross-sectional SEM image of the hierarchical ZnO film with a thickness of about 20 μm. As can be seen, the

hierarchical architectured ZnO film is basically uniform and highly ordered. As the reaction time increases to 24 h, it can be seen from Fig. 1d-1e that the 3D hierarchical nanostructure for the ZnO is well remained as in Fig. 1a-1b, while the diameter and average length of the radially distributed ZnO nanorods increase to 350-400 nm and 4-5 μm (aspect ratio ~ 12), respectively. Fig. 1f shows the cross-sectional SEM image of the hierarchical ZnO film with a thickness of about 50 μm, which is larger than 20 μm of thickness of the hierarchical ZnO film grown for 12 h.

For the growth of ZnO hierarchical nanostructures, it is found that the concentration of NaOH plays an essential role on the morphologies of the hierarchical ZnO structures. As the concentration of NaOH is 0.35 M (Fig. S1a-b), randomly grown ZnO nanostuctures grown for 12 h are made of pencil-like rods with typical diameter of about 0.7 μm and length of 5 μm. When the concentration of NaOH increases to 0.45 M, ZnO hierarchical bundles with a higher density of ZnO nanorods than that prepared under a concentration of 0.55 M NaOH can be obtained, as shown in Fig. S1c-d. As the amount of NaOH increases to 0.65 M, it can be seen from Fig. S1e-f that the products are composed of randomly distributed ZnO rod-like structures with diameter of 0.6 μm and an average length of 6 μm (aspect ratio ~ 10). Fig. S2 depicts the hierarchical ZnO nanostructres grown fro 24 h in the presence of 0.35, 0.45, 0.65 M NaOH, respectively, showing the similar results as present in Fig. S1.

Fig. 2a, 2c, 2e show the SEM images of 12 h grown hierarchical ZnO nanostructrues, hierarchical 8CdS/ZnO and 3CdSe-8CdS/ZnO hybrids (8CdS and 3CdSe represent 3 and 8 cycles growth of CdS and CdSe, respectively). The corresponding EDS spectra of the products are given in Fig. 2b, 2d, 2f, respectively, showing that the products are composed of Zn and O elements for hierarchical ZnO nanostructrues, Zn, O, Cd and S elements for 8CdS/ZnO hierarchical nanostructures, Zn, O, Cd, S, and Se elements for hierarchical 3CdSe-8CdS/ZnO hybrids, respectively. Compared with the pure hierarchical ZnO nanostructures, uniformly distributed CdS QDs and CdS-CdSe QDs are loaded on the surfaces of hierarchical ZnO nanostructures. For the phase components and microstructures of the synthesized products, XRD and transmission electron microscopy characterization was carried out, as described in the following Fig. 3-4.

The XRD patterns of the hierarchical ZnO nanostructrues, hierarchical 8CdS/ZnO and 3CdSe-8CdS/ZnO hybrids, are illustrated in Fig. 3a, 3b, 3c, respectively. The diffraction patterns of ZnO hierarchical structure are fitted well with the bulk hexagonal ZnO crystal phase. The diffraction peaks located at 31.6°, 34.3°, 36.2°, 47.5°, 56.6°, and 62.8°, can be observed in all patterns of the ZnO hierarchical structure, which well agrees with (100), (002), (101), (102), (110), and (103) planes of ZnO structure, respectively (JCPDS No.36-1451). Compared with the XRD patterns of the hierarchical ZnO pure film, three additional peaks are observed at 26.8°, 43.9°, and 52.1° in the diffraction pattern of 8CdS/ZnO hierarchical structure, which well agree with (111), (220), and (311) planes of

cubic CdS structure (JCPDS No.21-0829), respectively (Fig. 3b). In the XRD pattern of the 3CdSe-8CdS/ZnO hierarchical structures, the additional peaks at 25.4°, 29.4°, and 52.1°, correspond well with (111), (200) and (222) planes of CdSe (JCPDS No.65-2891). The X-ray diffraction results shown in Fig 3 is well agrees with the EDS spectra shown in Fig. 2.

The microstructure and crystal phase of CdS sensitized and CdS-CdSe QDs double sensitized ZnO hierarchical nanostructures were further investigated by TEM. Fig. 4a and 4b depict low- and high-magnification TEM images of the hierarchical 8CdS/ZnO hybrids, showing that the hierarchical ZnO nanostructures are covered by CdS QDs. The HRTEM lattice image for the CdS QDs in Fig. 4c suggests that the diameter of the CdS QDs is estimated to be 3-5 nm, and two sets of lattice spacing of 0.335 and 0.287 nm correspond well to the d-spacing of (111) and (200) planes of cubic CdS (JCPDS No.21-0829), respectively. Three diffraction rings in Fig. 4d of the electron diffraction pattern correspond to (100) plane of ZnO, and (220), (222) planes of CdS, respectively. Fig. 4e and 4f show the low- and high-magnification TEM images of hierarchical 8CdS-3CdSe/ZnO hybrids, in comparison with that of the 8CdS/ZnO hybrids, the QDs layer on surface of ZnO becomes thicker with the deposition of CdSe QDs. In the HRTEM lattice image of Fig. 4g, the spacing of 0.334 and 0.216 nm corresponds to the d-spacing of (111) plane of CdS (111), and d-spacing of (220) plane of CdSe, respectively. The diffraction rings in the electron diffraction pattern in Fig. 4h match well with (100) plane of ZnO, (220) plane of CdS, and (400) plane of CdSe, respectively. The results shown in Fig. 4 are in good agreement with the XRD patterns in Fig. 3. For the SEM images and XRD patterns of the Cu_2S counter electrodes, please see Fig. S3 and Fig. S4 in the Supporting Information.

3.2 Optical properties characterization

Optical absorption measurements are used to determine the optical response properties of the synthesized hierarchical ZnO, 8CdS/ZnO, and 3CdSe-8CdS/ZnO samples. Fig. 5a gives the UV-vis absorption spectra of hierarchical ZnO, 8CdS/ZnO, and 3CdSe-8CdS/ZnO hybrids. The absorption wavelength at 420 nm is very weak for pure ZnO hierarchical structure. Compared with pure ZnO hierarchical structure, the absorption edge of 8CdS/ZnO hierarchical structure shows a red shift to 450 nm, with a broad peak and higher intensity in visible region. After depositing CdSe QDs on 8CdS/ZnO hierarchical structures, the absorption peak of hierarchical 3CdSe-8CdS/ZnO hybrids red shifted to 470 nm, displaying enlarged light absorption region.

The band gap energy of the hierarchical hybrids can be confirmed roughly according to the plots in Fig. 5b, which is obtained via the transformation based on the function $(\alpha h\nu)^2 = K(h\nu - E_g)$, where α is the absorbance, $h\nu$ is the photon energy, and K is parameter.[56-58] The estimated band gap value of the hierarchical ZnO, hierarchical hybrids of 4CdS/ZnO, 8CdS/ZnO, 12CdS/ZnO, 3CdSe-8CdS/ZnO, corresponds approximately to the light

responsibility with an energy band gap of 3.35, 2.61, 2.52, 2.33 and 2.44 eV, respectively. Therefore, it can be concluded that the transition of light responsibility from UV to visible light of the hierarchical hybrids can be realized by the coupling of CdS and CdSe QDs with hierarchical ZnO nanostructures.

Photovoltaic activity is closely related with the lifetime of photogenerated electrons and holes. It is generally accepted that PL signals result from the recombination of photoinduced charge carriers.[59] To confirm the charge separation behavior and efficiency in ZnO hierarchical structure, we carried out PL measurements by a spectrophotometer containing a xenon lamp with 360 nm excitation wavelength. Generally, there are three PL peaks in the UV, green and yellow regions observed in ZnO. The UV emissions are commonly attributed to the direct recombination of excitons through an exciton-exciton collision process, where one of the excitons radiatively recombines to generate a photon (the exciton emission process). The green and yellow emissions are identified as being from the radiative recombination of the electrons from shallow donors with the trapped holes from singly ionized oxygen vacancies and interstitial oxygen.[60] Fig. 5c comparatively shows the PL spectra of pure hierarchical ZnO structure, CdS- and CdSe-CdS QDs sensitized ZnO hierarchical hybrids. All the samples displayed a broad-band emission from 450 to 650 nm with two similar emission peaks: 465, and 550 nm. We observed a very intense broad emission at 465 nm (Fig. 5c). Emissions in the visible range are generally considered to be induced by defects.[61,62] It is shown that the position of the emission peaks at 465 and 550 nm does not change. However, with the coupling of CdS and CdSe QDs with hierarchical ZnO structures, the emission peak intensity at 465 and 550 nm decreases, indicating lower recombination rate of photogenerated electrons and holes for the QDs sensitized hierarchical ZnO hybrids than that of the pure hierarchical ZnO.[63,64] The low recombination rate of photogenerated electrons and holes means more electrons can be transferred to the conduction band of ZnO from QDs, resulting in high photo-electrical conversion efficiency of QDSCs.

3.3 The performance of solar cell based on CdSe-CdS QDs sensitized ZnO hierarchical structure

The performance parameters of the soar cells including the short circuit current density (J_{sc}), open circuit potential (V_{oc}), fill factor (FF) and conversion efficiency (η) of all the solar cells are listed in Table 1. Fig. 6a comparatively depicts the photocurrent density-voltage (J-V) characteristics of 4-cycle CdS QDs sensitized 12 h and 24 h grown ZnO QDSCs cells (denoted as 4CdS/12h ZnO, 4CdS/24h ZnO hybrids) using Cu_2S as a counter electrode under the illumination of 1 sun (AM 1.5, 100 $mW \cdot cm^{-2}$), showing that 4CdS/12h ZnO hybrid cell displays better performance than 4CdS/24h ZnO hybrid cell. So the 12 h ZnO film with a thickness of about 20 μm is more applicable for the ZnO cells. The two cells display the same V_{oc} (0.49), 4CdS/24h ZnO has a larger J_{sc}, but 4CdS/12h ZnO has a larger FF, which results in a larger photo-electrical conversion efficiency (0.59) for 4CdS/12h

ZnO cell has than 4CdS/24h ZnO cell (0.46). So a larger film thickness of the working electrode may induce diminution of the FF, and then results in the decrease of energy conversion efficiency. The ZnO hierarchical structure electrode with a thickness of about 20 μm is enough to absorb QDs and produce electrons and holes, and can avoid hindering the absorption of light.

The photovoltaic performance of QDSCs based on CdS, CdSe sensitized 12 h grown hierarchical ZnO structure on ITO substrates is systematically evaluated in a photoelectrochemical cell. The J-V characteristics for QDSCs based on pure hierarchical ZnO, CdS, and CdSe-CdS double-sensitized ZnO hierarchical hybrids are shown in Fig 6b. For the QDSCs based on non-sensitized pure ZnO hierarchical structure (curve 12h ZnO in Fig 6b), the V_{OC} (0.15) and J_{sc} (1.12) are very low. For the QDSCs based on QDs sensitized hierarchical ZnO hybrids, it is generally believed that the solar performance gets improved with the increase in the thickness of the CdS QDs. However, a larger thickness of CdS QDs may induce diminution of the J_{sc}, and then results in the decrease of energy conversion efficiency.[65] It is shown that the 8 cycle growth of CdS on hierarchical ZnO (8CdS/ZnO) is the optimal parameter for obtaining improved solar cell performance of the QDs sensitized ZnO hybrids. The QDSCs based on 8CdS/ZnO perform better than 4CdS/ZnO hierarchical hybrids in terms of the V_{OC} and the J_{sc}, resulting in higher power conversion efficiency (0.87% for 8CdS QDs vs. 0.59% for 4CdS), which is attributed to the broader light absorption of 8CdS compared with that of 4CdS (Fig 5a).[66]

The additional layer deposition of CdSe QDs on the basis of 4CdS/ZnO hierarchical hybrids could further improve the photo-electrical conversion efficiency of the QDSCs. The best performance can be achieved for QDSCs based on QDs double sensitized 3CdSe-8CdS/ZnO ZnO hierarchical structures, showing a photo-electrical conversion efficiency of 1.39, with V_{OC} of 0.62 V and J_{SC} of 4.32 mA/cm^2, respectively. The performance characteristics of the solar cells illustrated in Fig 6b are summarized in Table 1. This shows an advantage of synergetic effects of two kinds of narrow band gap semiconductor QDs co-sensitizing wide gap semiconductor for QDSCs application, as has been discussed recently.[67,68]

Scheme 2 depicts the typical component for the solar cell based on CdSe-CdS QDs co-sensitized ZnO hierarchical structure. The photovoltaic device is composed of the CdSe-CdS QDs loaded hierarchical ZnO photoanode and Cu_2S-counter electrode assembled into a sandwich type cell, a liquid redox electrolyte consisted of 1 M Na_2S, 1 M S and 0.5 M NaOH in pure ethanol. During operation, photons are captured by QDs, yielding electron-hole pairs that are rapidly separated to electrons and holes at the interface between the ZnO and the QDs. The electrons inject into the oxide film (ZnO) and the holes are released by redox couples in the liquid polysulfide (S^{2-}/S_x^{2-}) electrolyte.

3.4 Electrochemical impedance spectroscopy (EIS) analysis

In order to better understand the kinetics of electrochemical and photoelectrochemical processes occurring in QDSCs, the analysis of electrochemical impedance spectroscopy (EIS) of the QDSCs noted above was performed under illumination and open-circuit voltage. Fig. 7 shows the Nyquist plots of QDSCs based on hierarchical 8CdS/ZnO and 3CdSe-8CdS/ZnO hybrids. Both of them have two semicircles with a contact series resistance (Rs) on the ITO substrate. An equivalent circuit containing a constant phase element (CPE) and resistances (R) (see the inset of Fig. 7) was used to fit the Nyquist plots to estimate the electron transport parameters,[69] such as Rs: series resistance，R_{CE}: charge-transfer resistance at the counter electrode-electrolyte interface, $R_{rec\text{-}ZnO}$: recombination resistance at the photoanode-electrolyte interface, C_{CE}: double-layer capacitance at the counter electrode, C_{ZnO}: chemical capacitance of ZnO photoanode. The fitted values listed in Table 2, where the electron lifetime can be estimated by $\tau_n' = R_{rec\text{-}ZnO} \times C_{ZnO}$.[22] The cells based on the 8CdS/ZnO and 3CdSe-CdS/ZnO posses the same Rs of 14.3 Ω and similar R_{CE} of 129.8 Ω, and 115.6 Ω, respectively, due to the use of the same counter electrode (Cu_2S) and electrolyte(S^{2-}/S_x^{2-}). However, the recombination resistance ($R_{rec\text{-}ZnO}$) of the 8CdSZnO (346.1 Ω) is larger than that of the 3CdSe-CdS/ZnO (249.2 Ω), implying a slower electron recombination process for the former, which is in agreement with the higher open-circuit. The electron lifetimes τ_n' of these QDSSCs calculated by EIS showed the same order. Table 2 shows the electrochemical impedance results of QDSCs.

4 Conclusions

We have developed a simple method of fabricating ZnO/CdS/CdSe QDSCs by combining hydrothermal method and SILAR techniques sequentially. The method consists of the growth of ZnO hierarchical structure on ITO substrates by hydrothermal method and the decorattion of double quantum dots CdSe and CdS by SILAR. A CdS/CdSe QDs layer was formed uniformly along the ZnO hierarchical structure. The double-sensitized ZnO hierarchical structures show enhanced light absorption in entire visible light range. As photoanodes in QDSCs, the double-sensitized ZnO hierarchical structure demonstrated an increased J_{sc} and an improved power conversion efficiency up to 1.39%. During light illumination, photons are captured by QDs, yielding electron-hole pairs that are rapidly separated to electrons and holes at the interface between the ZnO and the QDs. The electrons inject into the oxide film (ZnO) and the holes are released by redox couples in the liquid polysulfide (S^{2-}/S_x^{2-}) electrolyte. The results suggest that it is very promising and feasible to enhance light absorption, carrier generation, and effective carrier separation via band engineering by double sensitization, and the method reported here has a great potential to be scaled up.

Acknowledgements

We acknowledge support from the National Natural Science Funds (No. 51272137, 51025211), The National Basic Research Program (No: 2013CB934303), the Tai Shan Scholar Foundation of Shandong Province.

References

1. B. O'regan and M. Grfitzeli, *nature,* 1991, **353**, 737-740.
2. C. J. Barbe, F. Arendse, P. Comte, M. Jirousek, F. Lenzmann, V. Shklover and M. Grätzel, *J. Am. Ceram. Soc.,* 1997, **80**, 3157-3171.
3. A. Yella, H. W. Lee, H. N. Tsao, C. Yi, A. K. Chandiran, M. K. Nazeeruddin, E. W. Diau, C. Y. Yeh, S. M. Zakeeruddin and M. Gratzel, *Science,* 2011, **334**, 629-634.
4. Q. Zhang and G. Cao, *Nano Today* 2011, **6**, 91-109.
5. T. Bessho, E. Yoneda, J.-H. Yum, M. Guglielmi, I. Tavernelli, H. Imai, U. Rothlisberger, M. K. Nazeeruddin and M. Grätzel, *J. Am. Chem. Soc.,* 2009, **131**, 5930-5934.
6. P. G. Bomben, K. C. Robson, P. A. Sedach and C. P. Berlinguette, *Inorg. Chem.,* 2009, **48**, 9631-9643.
7. P. G. Johansson, J. G. Rowley, A. Taheri, G. J. Meyer, S. P. Singh, A. Islam and L. Han, *Langmuir,* 2011, **27**, 14522-14531.
8. H. C. Zhao, J. P. Harney, Y. T. Huang, J. H. Yum, M. K. Nazeeruddin, M. Gratzel, M. K. Tsai and J. Rochford, *Inorg. Chem.,* 2012, **51**, 1-3.
9. J. Kim, H. Choi, C. Nahm, J. Moon, C. Kim, S. Nam, D.-R. Jung and B. Park, *J. Power Sources,* 2011, **196**, 10526-10531.
10. S. Panigrahi and D. Basak, *J. Colloid Interface Sci.,* 2011, **364**, 10-17.
11. I. Robel, V. Subramanian, M. Kuno and P. V. Kamat, *J. Am. Chem. Soc.,* 2006, **128**, 2385-2393.
12. Q. Shen, J. Kobayashi, L. J. Diguna and T. Toyoda, *J. Appl. Phys.,* 2008, **103**, 084304-5.
13. R. Plass, S. Pelet, J. Krueger, M. Grätzel and U. Bach, *J. Phys. Chem. B,* 2002, **106**, 7578-7580.
14. P. Yu, K. Zhu, A. G. Norman, S. Ferrere, A. J. Frank, and A. J. Nozik, *J. Phys. Chem. B,* 2006, **110**, 25451-25454.
15. A. Nozik, *Physica E,* 2002, **14**, 115-120.
16. P. V. Kamat, *J. Phys. Chem. C,* 2008, **112**, 18737-18753.
17. G. Hodes, *The J. Phys. Chem. C,* 2008, **112**, 17778-17787.
18. W. U. Huynh, J. J. Dittmer, A. P. Alivisatos, *Science,* 2002, **295**, 2425-2427.
19. R. Schaller and V. Klimov, *Phys. Rev. Lett.,* 2004, **92**, 186601-4.
20. M. Shalom, I. Hod, Z. Tachan, S. Buhbut, S. Tirosh and A. Zaban, *Energy Environ. Sci.,* 2011, **4**, 1874-1878.
21. S. H. Im, H.-j. Kim, S. W. Kim, S.-W. Kim and S. I. Seok, *Energy Environ. Sci.,* 2011, **4**, 4181-4186.
22. I. Mora-Seró, S. Giménez, F. Fabregat-Santiago, R. Gómez, Q. Shen, T. Toyoda and J. Bisquert, *Accounts Chem. Res.,* 2009, **42**, 1848-1857.
23. S. Buhbut, S. Itzhakov, E. Tauber, M. Shalom, I. Hod, T. Geiger, Y. Garini, D. Oron and A. Zaban, *ACS Nano,* 2010, **4**, 1293-1298.
24. L. M. Peter, K. U. Wijayantha, D. J. Riley and J. P. Waggett, *J. Phys. Chem. B,* 2003, **107**, 8378-8381.
25. E. C. Garnett and P. Yang, *J. Am. Chem. Soc.,* 2008, **130**, 9224-9225.
26. M. Law, L. E. Greene, J. C. Johnson, R. Saykally and P. Yang, *Nature Mater.,* 2005, **4**, 455-459.
27. K. Ariga, A. Vinu, Y. Yamauchi, Q. Ji and J. P. Hill, *Bull. Chem. Soc. Jpn.,* 2012, **85**, 1-32.
28. Y. Liu, J. Goebl and Y. Yin, *Chem.Soc.Rev.,* 2013, **42** (7), 2610-2653.
29. Z. Sun, T. Liao, Y. Dou, S. M. Hwang, M.-S. Park, L. Jiang, J. H. Kim and S. X. Dou, Nat. Commun., 2014, **5**.
30. K. Ariga, Y. Yamauchi, G. Rydzek, Q. Ji, Y. Yonamine, K. C.-W. Wu and J. P. Hill, *Chem. Lett.,* 2014, **43**, 36-68.
31. J.-G. Kim, D. Shi, M.-S. Park, G. Jeong, Y.-U. Heo, M. Seo, Y.-J. Kim, J. H. Kim and S. X. Dou, *Nano Res.,* 2013, **6**, 365-372.
32. J. G. Kim, M. S. Park, S. M. Hwang, Y. U. Heo, T. Liao, Z. Sun, J. H. Park, K. J. Kim, G. Jeong and Y. J. Kim, *ChemSusChem,* 2014, **7**, 1451-1457.
33.A. Kongkanand, K. Tvrdy, K. Takechi, M. Kuno and P. V. Kamat, *J. Am. Chem. Soc.,* 2008, **130**, 4007-4015.
34. K. S. Leschkies, R. Divakar, J. Basu, E. Enache-Pommer, J. E. Boercker, C. B. Carter, U. R. Kortshagen, D. J. Norris and E. S.

Aydil, *Nano Lett.,* 2007, **7**, 1793-1798.

35. Y.-J. Lee, D. S. Ruby, D. W. Peters, B. B. McKenzie and J. W. Hsu, *Nano Lett.,* 2008, **8**, 1501-1505.

36. G. Hodes, J. Manassen and D. Cahen, *J. Electrochem. Soc.,* 1980, **127**, 544-549.

37. Z. Yang, C. Y. Chen, C. W. Liu and H. T. Chang, *Chem. Commun.,* 2010, **46**, 5485-5487.

38. Z. Yang, C. Y. Chen, C. W. Liu, C. L. Li and H. T. Chang, *Adv. Energy Mater.,* 2011, **1**, 259-264.

39. S. Gimenez, I. Mora-Sero, L. Macor, N. Guijarro, T. Lana-Villarreal, R. Gomez, L. J. Diguna, Q. Shen, T. Toyoda and J. Bisquert, *Nanotechnology,* 2009, **20**, 295204-6.

40. V. González-Pedro, X. Xu, I. Mora-Sero and J. Bisquert, *ACS nano,* 2010, **4**, 5783-5790.

41. S.-R. Jang, R. Vittal and K.-J. Kim, *Langmuir,* 2004, **20**, 9807-9810.

42. K. Imoto, K. Takahashi, T. Yamaguchi, T. Komura, J.-i. Nakamura and K. Murata, *Sol. Energ. Mat. Sol. C.,* 2003, **79**, 459-469.

43. T. N. Murakami, S. Ito, Q. Wang, M. K. Nazeeruddin, T. Bessho, I. Cesar, P. Liska, R. Humphry-Baker, P. Comte, P. t. Péchy and M. Grätzel, *J. Electrochem. Soc.,* 2006, **153**, A2255-A2261.

44. B. Fang, S. Q. Fan, J. H. Kim, M. S. Kim, M. Kim, N. K. Chaudhari, J. Ko and J. S. Yu, *Langmuir,* 2010, **26**, 11238-11243.

45. Y. Tak, S. J. Hong, J. S. Lee and K. Yong, *J. Mater. Chem.,* 2009, **19**, 5945.

46. X. Wang, H. Zhu, Y. Xu, H. Wang, Y. Tao, S. Hark, X. Xiao and Q. Li, *ACS nano,* 2010, **4**, 3302-3308.

47. N. Guijarro, T. Lana-Villarreal, I. Mora-Seró, J. Bisquert and R. Gómez, *J. Phys. Chem. C,* 2009, **113**, 4208-4214.

48. L. Liu, J. Hensel, R. C. Fitzmorris, Y. Li and J. Z. Zhang, *J. Phys. Chem. Lett.,* 2009, **1**, 155-160.

49. M. Seol, H. Kim, Y. Tak and K. Yong, *Chem. Commun.,* 2010, **46**, 5521-5523.

50. G. Wang, X. Yang, F. Qian, J. Z. Zhang, Y. Li, *Nano Lett.,* 2010, **10**, 1088-92.

51. C.-H. Chang and Y.-L. Lee, *Appl. Phys. Lett.,* 2007, **91**, 053503.

52. H. Lee, M. Wang, P. Chen, D. R. Gamelin, S. M. Zakeeruddin, M. Grätzel and M. K. Nazeeruddin, *Nano Lett.,* 2009, **9**, 4221-4227.

53.J. H. Bang and P. V. Kamat, *ACS Nano,* 2009, **3**, 1467-76.

54. X. Zhang, T. Chen, H.-J. Yan, D. Wang, Q.-H. Fan, L.-J. Wan, K. Ghosh, H.-B. Yang and P. J. Stang, *ACS nano,* 2010, **4**, 5685-5692.

55. R. Shi, P. Yang, J. Wang, A. Zhang, Y. Zhu, Y. Cao and Q. Ma, *CrystEngComm,* 2012, **14**, 5996.

56. H. Wei, S. Chen, X. Ren, B. Qian, Y. Su, Z. Yang and Y. Zhang, *CrystEngComm,* 2012, **14**, 7408.

57. G. Jeong, J.-G. Kim, M.-S. Park, M. Seo, S. M. Hwang, Y.-U. Kim, Y.-J. Kim, J. H. Kim and S. X. Dou, *ACS Nano,* 2014, **8**, 2977-2985.

58. J. Tauc, R. Grigorovici and A. Vancu, *Phys. Stat. Sol.,* 1966, **15**, 627-637.

59. J. Liqiang, Q. Yichun, W. Baiqi, L. Shudan, J. Baojiang, Y. Libin, F. Wei, F. Honggang and S. Jiazhong, *Sol. Energ. Mat. Sol. C,.* 2006, **90**, 1773-1787.

60. X. L. Wu, G. G. Siu, C. L. Fu and H. C.Ong, *Appl. Phys. Lett.,* 2001, **78**, 2285.

61. E. Erdem, J. Alloys. Compd., 2014, **605**, 34-44.

62. H. Kaftelen, K. Ocakoglu, R. Thomann, S. Tu, S. Weber and E. Erdem, Phys. Rev. B, 2012, **86**, 014113.

63. J. Hu, X. Ma, Z. Xie, N. Wong, C. Lee and S. Lee, *Chem. Phys. Lett.,* 2001, **344**, 97-100.

64. Z. Fu, B. Lin, G. Liao and Z. Wu, *J. Cryst. Growth,* 1998, **193**, 316-321.

65. Y. Shengyuan, A. S. Nair, R. Jose and S. Ramakrishna, *Energy Environ. Sci.,* 2010, **3**, 2010.

66. C. Luan, A. Vaneski, A. S. Susha, X. Xu, H. E. Wang, X. Chen, J. Xu, W. Zhang, C. S. Lee, A. L. Rogach and J. A. Zapien, *Nanoscale Res. Lett.,* 2011, **6**, 340.

67. I. Mora-Seró and J. Bisquert, *J. Phys. Chem. Lett.,* 2010, **1**, 3046-3052.

68. Y.-L. Lee and Y.-S. Lo, *Adv. Funct. Mater.,* 2009, **19**, 604-609.

69. C. Zha, L. Shen, X. Zhang, Y. Wang, B. A. Korgel, A. Gupta and N. Bao, *ACS Appl. Mater. Interfaces,* 2014, **6**, 122-129.

Figure Captions

Scheme 1. Deposition process of CdS and CdSe QDs on ZnO/ITO film using successive ionic layer adsorption and reaction (SILAR) method.

Fig. 1 Typical SEM images of ZnO prepared on ITO substrate with 0.55 M NaOH in different reaction time. (a, b) 12h (c) Cross-sectional SEM images of ZnO, 12h; (d, e) 24 h (f) Cross-sectional SEM images of ZnO, 24 h.

Fig. 2 SEM images of (a) 12h ZnO, (c) 8CdS/12h ZnO, and (e) 3CdSe-8CdS/12h ZnO prepared on ITO substrate. EDS spectra of (b) 12h ZnO, (d) 8CdS/12h ZnO, and (f) 3CdSe-8CdS/12h ZnO.

Fig. 3 XRD patterns of (a)12h ZnO, (b)8CdS/12h ZnO, and (c)3CdSe-8CdS/12h ZnO.

Fig. 4 (a, b) TEM, (c) HR-TEM images and (d) SAED spectrum of as-synthesized 8CdS/ZnO hierarchical structure, (e, f) TEM, (g) HR-TEM images and (h) SAED spectrum of as-synthesized 3CdSe-8CdS/ZnO hierarchical structure.

Fig. 5 (a) Absorption spectra of ZnO, CdS/ZnO, and CdSe-CdS/ZnO hierarchical structure. (b) Plots of $(ahv)^2$ versus the photon energy (hv) reveal the Eg of ZnO, CdS/ZnO, and CdSe-CdS/ZnO hierarchical structure. (c) PL spectra of ZnO, CdS/ZnO, and CdSe-CdS/ZnO hierarchical structure.

Fig 6 J-V curves of the QDSCs based on (a) 4CdS/12h ZnO and 4CdS/24h ZnO, and (b) the ZnO, CdS/ZnO, and CdSe-CdS/ZnO.

Fig. 7 Nyquist impedance plots of under one-sun irradiation of 8CdS/ZnO and 3CdSe-8CdS/ZnO QDSCs. The inset shows the equivalent circuit used to obtain the fitted curves (solid lines) by fitting the experimental data (dots). All measurements were done under simulated AM1.5 solar light (100 mW cm^{-2}). The frequency range was 10 mHz to 100 KHz; the magnitude of the alternating potential was 10 mV.

Scheme 2. Sketch of the photoelectrical conversion structure of QDSCs.

Table 1 Photovoltaic parameters of the assembled devices.

Table 2 Simulated values of resistance (R) and capacitance (C) of EIS spectra calculated by equivalent circuit as shown in Fig. 7. The electron lifetimes τ_n' are estimated by $R_{rec\text{-}ZnO}$ and C_{ZnO} electrochemical impedance results of QDSCs.

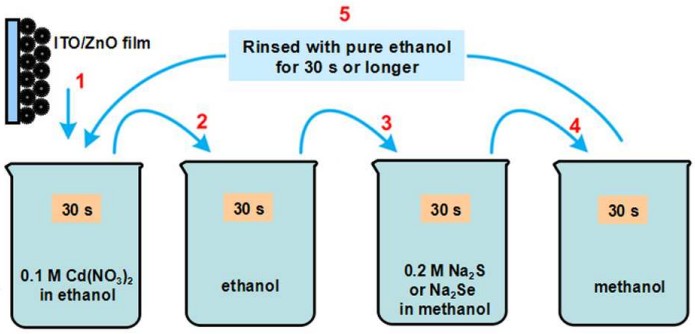

Scheme 1. Deposition process of CdS and CdSe QDs on ZnO/ITO film using successive ionic layer adsorption and reaction (SILAR) method.

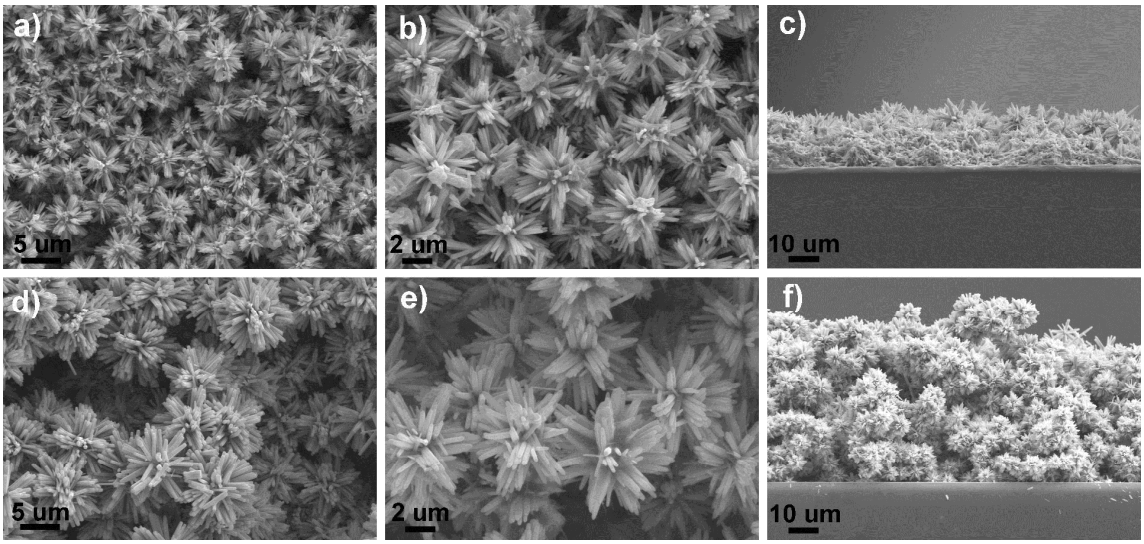

Fig. 1 Typical SEM images of ZnO prepared on ITO substrate with 0.55 M NaOH in different reaction time. (a, b) 12h (c) Cross-sectional SEM images of ZnO, 12h; (d, e) 24 h, (f) Cross-sectional SEM images of ZnO, 24 h.

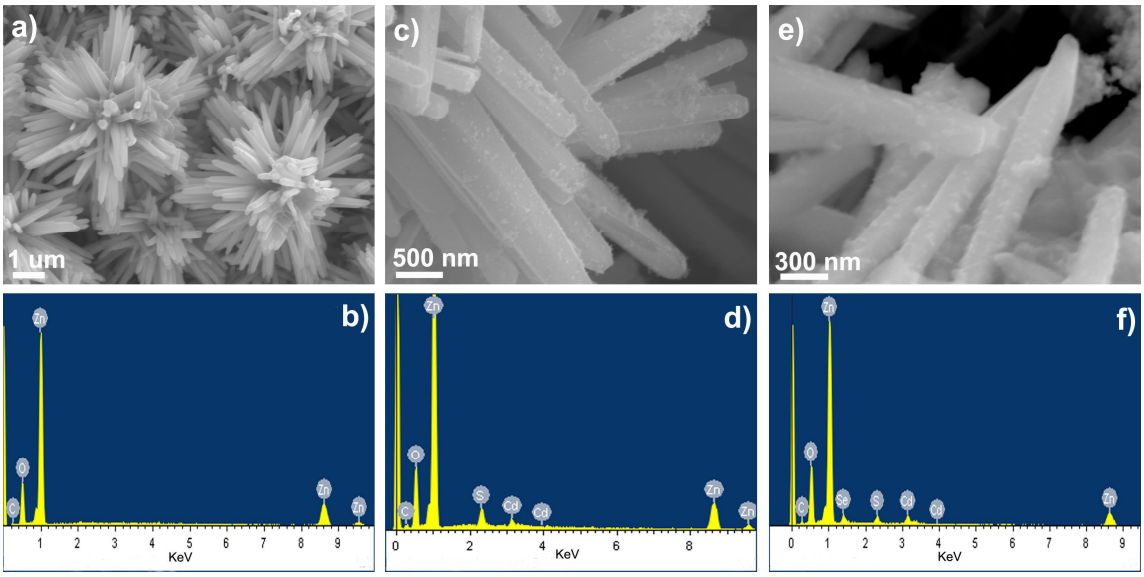

Fig. 2 SEM images of (a) 12h ZnO, (c) 8CdS/12h ZnO, and (e) 3CdSe-8CdS/12h ZnO prepared on ITO substrate. EDS spectra of (b) 12h ZnO, (d) 8CdS/12h ZnO, and (f) 3CdSe-8CdS/12h ZnO

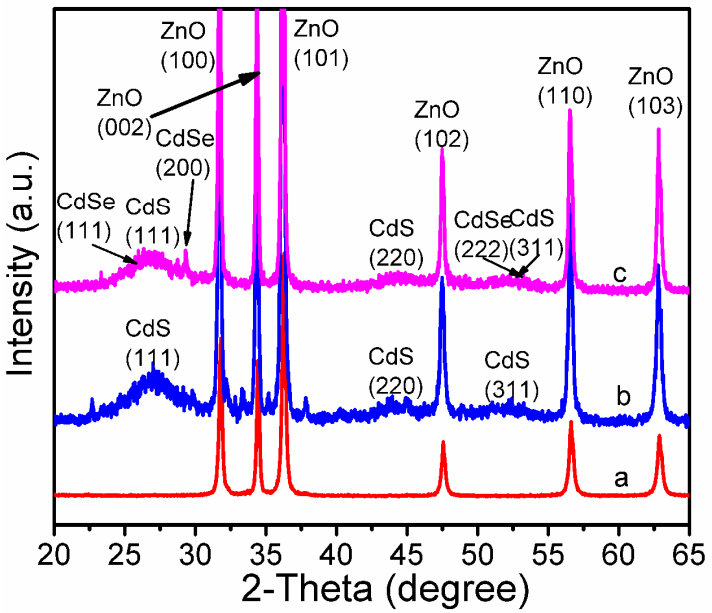

Fig. 3 XRD patterns of (a) 12h ZnO, (b) 8CdS/12h ZnO, and (c) 3CdSe-8CdS/12h ZnO

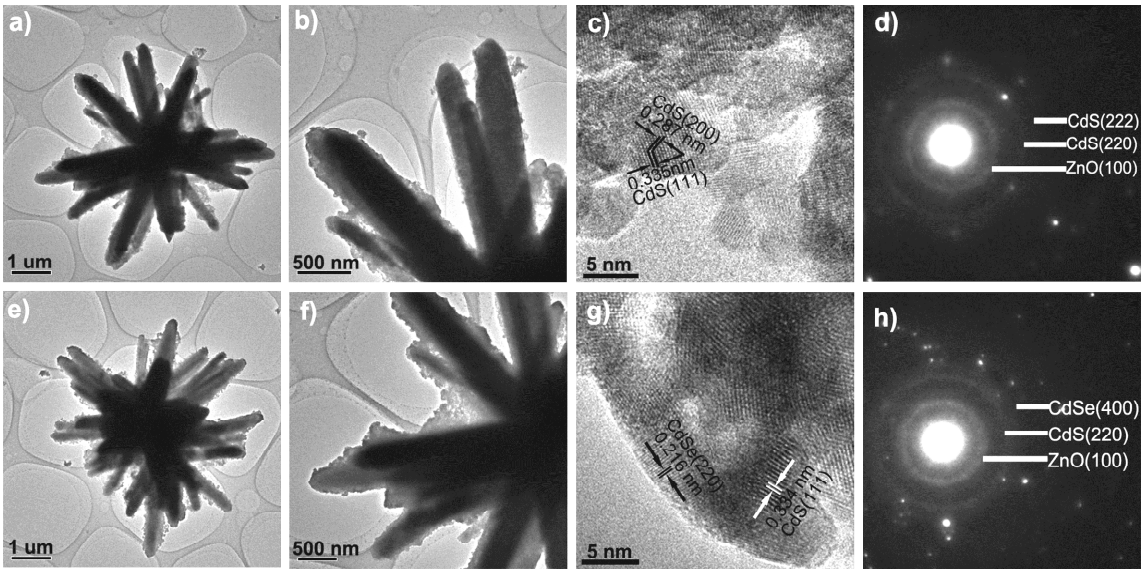

Fig. 4 (a, b) TEM, (c) HR-TEM images and (d) SAED spectrum of as-synthesized 8CdS/ZnO hierarchical structure, (e, f) TEM, (g) HR-TEM images and (h) SAED spectrum of as-synthesized 3CdSe-8CdS/ZnO hierarchical structure.

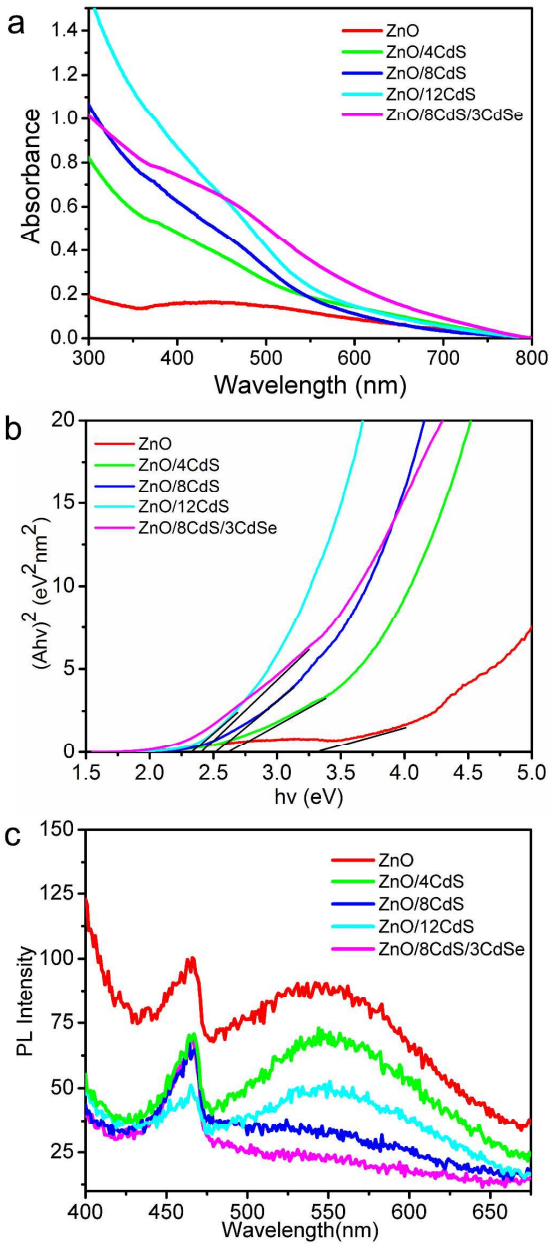

Fig. 5 (a) Absorption spectra of ZnO, CdS/ZnO, and CdSe-CdS/ZnO hierarchical structure. (b) Plots of $(ahv)^2$ versus the photon energy (hv) reveal the Eg of ZnO, CdS/ZnO, and CdSe-CdS/ZnO hierarchical structure. (c) PL spectra of ZnO, CdS/ZnO, and CdSe-CdS/ZnO hierarchical structure.

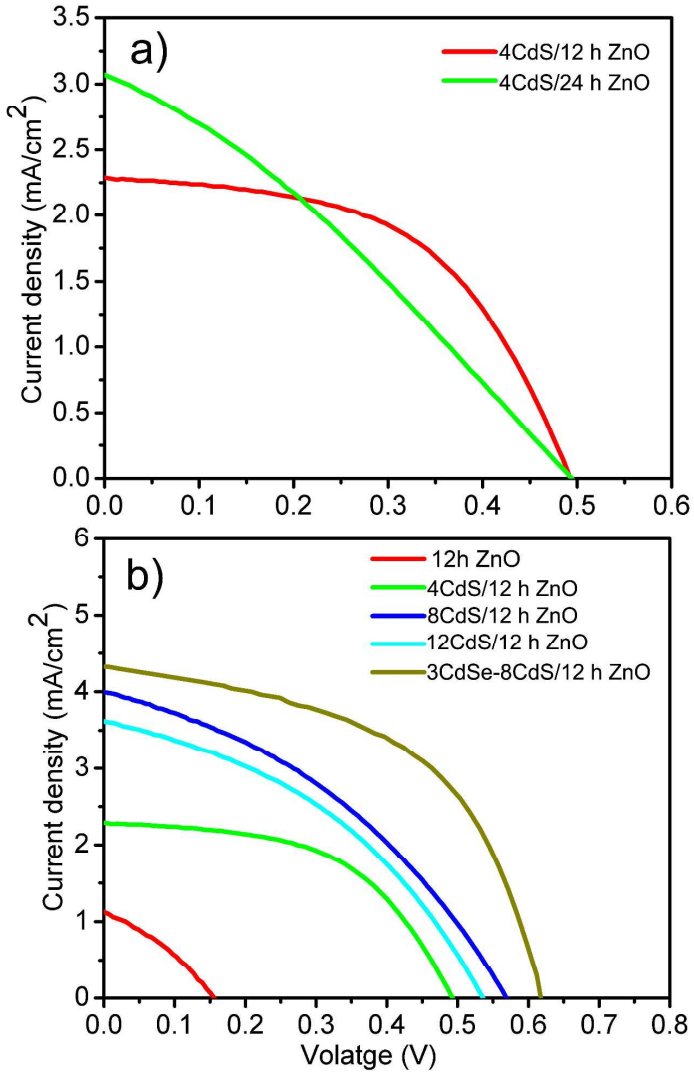

Fig 6 J-V curves of the QDSCs based on (a) the 4CdS/12h ZnO and 4CdS/24h ZnO, and (b) the ZnO, CdS/ZnO, and CdSe-CdS/ZnO.

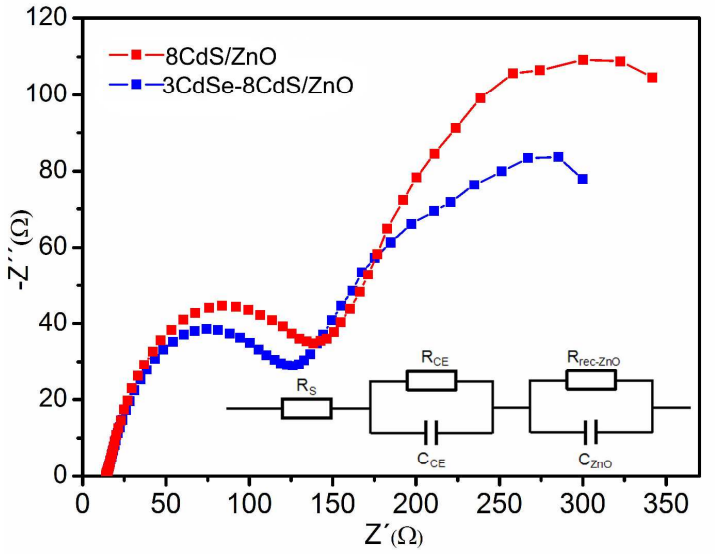

Fig. 7 Nyquist impedance plots of under one-sun irradiation of 8CdS/ZnO and 3CdSe-8CdS/ZnO QDSCs. The inset shows the equivalent circuit used to obtain the fitted curves (solid lines) by fitting the experimental data (dots). All measurements were done under simulated AM1.5 solar light (100 mW cm-2). The frequency range was 10 mHz to 100 KHz; the magnitude of the alternating potential was 10 mV.

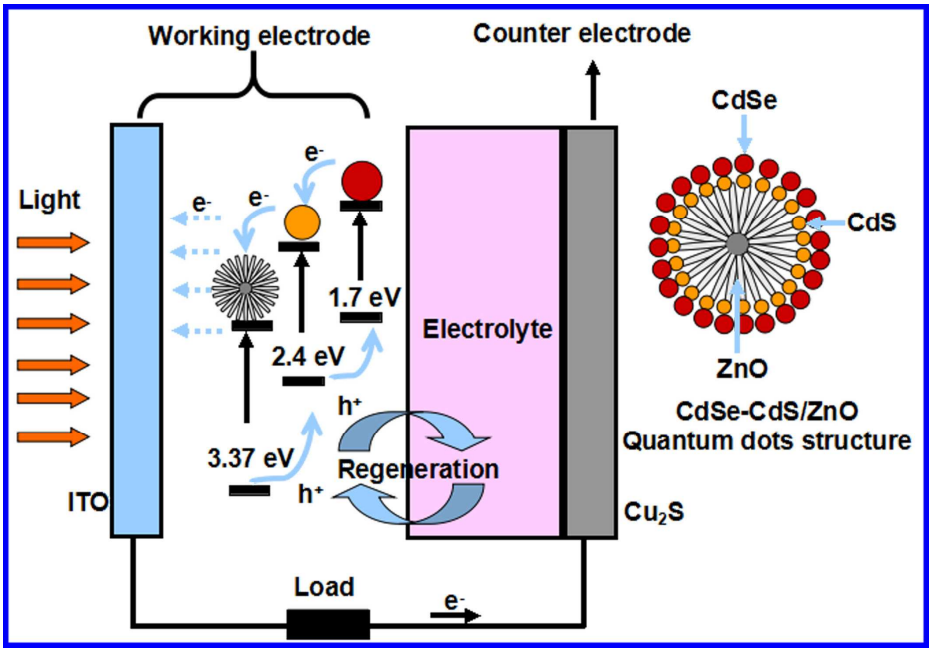

Scheme 2. Sketch of the photoelectrical conversion structure of QDSCs.

Table 1 Photovoltaic parameters of the assembled devices

Devices	Counter	J_{sc}(mA/cm^2)	V_{oc}(V)	FF(%)	η(%)
12 h ZnO	Cu_2S	1.12	0.15	33.16	0.04
4CdS/24h ZnO	Cu_2S	3.07	0.49	30.53	0.46
4CdS/12h ZnO	Cu_2S	2.29	0.49	52.86	0.59
8CdS/12h ZnO	Cu_2S	4.01	0.57	37.98	0.87
12CdS/12h ZnO	Cu_2S	3.63	0.53	39.85	0.77
3CdSe-8CdS/12h ZnO	Cu_2S	4.32	0.62	52.98	1.39

Table 2 Simulated values of resistance (R) and capacitance (C) of EIS spectra calculated by equivalent circuit as shown in Fig. 7. The electron lifetimes τ_n' are estimated by $R_{rec\text{-}ZnO}$ and C_{ZnO} electrochemical impedance results of QDSCs.

Devices	R_s(Ω)	R_{CE}(Ω)	C_{CE}(μF)	$R_{rec\text{-}ZnO}$(Ω)	C_{ZnO}(μF)	τ_n'(ms)
8CdS/12 h ZnO	14.3	129.8	0.5	346.1	17.7	6.1
3CdSe-8CdS/12 h ZnO	14.3	115.6	0.5	249.2	18.9	4.7